

The Hartree-Fock phase diagram of the two-dimensional electron gas

B. Bernu,¹ F. Delyon,² M. Holzmann,^{1,3} and L. Baguet¹

¹*LPTMC, UMR 7600 of CNRS, Université P. et M. Curie, Paris, France*

²*CPHT, UMR 7644 of CNRS, École Polytechnique, Palaiseau, France*

³*Univ. Grenoble 1/CNRS, LPMMC UMR 5493, Maison des Magistères, 38042 Grenoble, France*
(Dated: May 17, 2022)

We calculate the ground state phase diagram of the homogeneous electron gas in two dimensions within the Hartree-Fock approximation. At high density, we find stable solutions, where the electronic charge and spin density form an incommensurate crystal having more crystal sites than electrons, whereas the commensurate Wigner crystal is favored at lower densities, $r_s \gtrsim 1.22$. Our explicit calculations demonstrate that the homogeneous Fermi liquid state – though being an exact stationary solution of the Hartree-Fock equations – is never the Hartree-Fock ground state of the electron gas.

PACS numbers: 71.10.-w, 71.10.Ca, 71.10.Hf, 71.30.+h, 03.67.Ac

I. INTRODUCTION

Electrons are found everywhere in matter, most of the time localized by positive charges. In typical condensed matter situations, electronic densities and temperatures are such that, in addition to the external positive charges, a quantum description of electrons interacting with each other is necessary, leading in general to a difficult quantum many-body problem. The homogeneous electron gas, where the positive charges are reduced to solely ensure global electro-neutrality, is one of the most fundamental model to study electronic correlation effects. In three dimensions, $d = 3$, valence electrons in alkaline metals realize the electron gas to high precision, in particular in solid sodium¹, whereas the two dimensional electron gas, $d = 2$, (2DEG) is relevant for electrons at heterostructures, e.g. semiconductor-insulator interfaces². At zero temperature, the electron gas is described by a single parameter, the density n or equivalently by the dimensionless parameter $r_s = a/a_B$. Here $a = [2(d-1)\pi n/d]^{-1/d}$ is the mean inter particle distance, and $a_B = \hbar^2/(me^2)$ is the Bohr radius, where $-e$ and m are the electronic charge and mass, respectively.

As pointed out by Wigner³, at low densities and zero temperature, electrons will form a crystal, supposed to melt at higher densities where the kinetic energy dominates over the interaction. In the limit $r_s \rightarrow 0$, the Hartree-Fock approximation (HF) applies. Since the non-interacting Fermi sea remains a stationary solution of the Hartree-Fock equations, it is natural to assume a Fermi liquid phase at high densities. First principle calculations, such as Quantum Monte Carlo⁴⁻⁷, have located the transition from the Wigner crystal (WC) to the homogeneous Fermi liquid (FL) to high precision. Still, there are indications that the Fermi liquid phase is not necessarily the absolute ground state of the electron gas at high densities⁸⁻¹⁰ and that a direct transition between Wigner crystal and a homogeneous Fermi liquid cannot occur in two dimensions^{11,12}. These conjectures actually hold already for the electron gas in the Hartree-Fock approximation, but, despite the early predictions by Overhauser of the spin and charge density instability of the Fermi liquid ground state, explicit, numerical HF calculations¹³ have not confirmed them for a long time. Only recently, the first self consistent Hartree-Fock solutions below the Fermi liquid energy have been found at high densities^{10,14}.

Previous HF calculations¹⁰ have shown that the fully polarized electron gas in two dimensions forms a charge density wave with triangular symmetry at high densities. In contrast to the low-density Wigner crystal, the number of maxima of the charge density wave is higher than the number of electrons, having thus metallic character, and we will refer to such states as incommensurate crystals in the following. However, incommensurate states give rise to important size effects, and the calculations in Ref. ¹⁰ were limited to ~ 500 electrons.

In this paper, we show how the incommensurate states can be represented by the vector Q of the charge modulation which simplifies the structure of the wave function. Restricting the search for the HF ground state to states with arbitrary Q , we are able to overcome size restrictions and we explore the phase diagram of the unpolarized and fully polarized electron gas, including triangular and square symmetries. We show that the incommensurate crystal is favored also in the unpolarized gas at high densities. Whereas the momentum distribution of the Wigner crystal is a continuous function of the momentum, we show that there are angle-selective steps in the incommensurate phase.

II. METHODS

A. Hamiltonian

The Hamiltonian of the electron gas containing N electrons writes

$$H = -\frac{1}{2} \sum_i \Delta_i + \sum_{1 \leq i < j \leq N_p} v(x_i - x_j) \quad (1)$$

where Δ_i is the Laplacian with respect to x_i , $v(x)$ is the electrostatic interaction $v(x) = \|x\|^{-1}$, and we have used atomic units where distances are measured in units of a_B and energies in Hartree, $1\text{Ha} = \hbar^2/(ma_B^2)$. In addition to Eq. (1), the interaction between electrons and a positive background charge must be considered to ensure charge neutrality.

We are considering N electrons in a finite box of volume V , of sizes L_1 and L_2 , with periodic boundary conditions, so that the momentum k belongs to the lattice L^* generated by L_1^* and L_2^* satisfying $L_i L_j^* = 2\pi \delta_{ij}$. Introducing the Fermi level k_F defined from $\pi k_F^2 = (1/2 + \zeta/2)N \det(L_1^*, L_2^*) = (1/2 + \zeta/2)N(2\pi)^2/V$, corresponding to the unpolarized ($\zeta = 0$) or completely polarized gas ($\zeta = 1$), and expressing the density $n = N/V$ in terms of r_s , we have $k_F a_B = (2 + 2\zeta)^{1/2}/r_s$. In the following, we express all momenta in units of k_F .

Within the Hartree-Fock approximation, the energy expectation value is minimized with respect to a single skew-symmetric product of N single particle states. Periodic solutions are special cases which can be described by Bloch waves, $|\varphi_k\rangle = \sum_{q \in \Lambda} a_k(q) |k + q\rangle$, where the periodic structure introduces a sub-lattice Λ in the momentum space

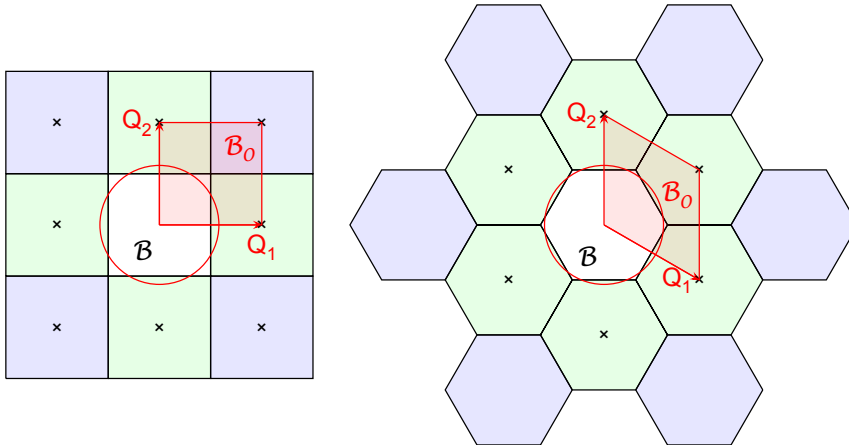


FIG. 1. (color on line) Illustration of the k -space in the square (left) and triangular (right) geometry. At the center of each figure, are shown the brillouin zone \mathcal{B} (in white) and the corresponding basis vectors Q_1 and Q_2 . The first and second shell of neighboring cells, $\mathcal{B} + n_1 Q_1 + n_2 Q_2$, are shaded in light-green and light blue, respectively. For square (resp. triangular) symmetry, the integers n_i of the first and second shell satisfy $n_1^2 + n_2^2 = 1, 2$ (resp. $n_1^2 + n_2^2 - n_1 n_2 = 1, 3$). Most of the results presented in this paper are done including a number of bands, M_Λ , which corresponds to two neighboring shells for the square and one for the triangular geometry. In light-red, we indicate the elementary cell, \mathcal{B}_0 , used in our numerical calculations. The circle indicates the spherical Fermi surface of a Fermi gas.

and k is chosen in the Brillouin zone, \mathcal{B} (see Fig.1). The Brillouin zone of a Wigner crystal (WC) contains exactly the same number of states as electrons, N , and an upper bound of the ground state energy is obtained minimizing the coefficients $a_k(q)$ of the Bloch functions. However, as r_s approaches zero, the kinetic energy dominates which is minimized by a circular density of occupied states, the Fermi gas (FG). Restricting the variational freedom of the HF calculations to FG and WC phases¹³, a discontinuous transition between FG and WC necessarily arises at a finite density since the Brillouin zone of the Wigner crystal cannot approach continuously the circular shape of the Fermi gas. In Ref.¹⁰, the HF energy of the polarized gas has been minimized without imposing periodicity of the solutions. At high densities, ground states of lower energy than FG and WC have been found leading to periodic solutions which are not commensurate with the number of electrons. These new solutions correspond to Bloch states where the Brillouin zone does not fit the number of particles, and, at the same time, the occupation of Bloch states of given k in the Brillouin zone can be different from one.

B. Representation of periodic states

For the periodic gas, the lattice Λ is a \mathbb{Z} -module generated by Q_1 and Q_2 in L^* (see Fig.1). For any chosen discretization M , we represent numerically the Brillouin zone with the set of vectors:

$$\mathcal{B}_0 = \{k \in \mathbb{R}^2; k = (n_1 Q_1 + n_2 Q_2)/M, 0 \leq n_i < M\}$$

For any $k \in \mathcal{B}_0$ we set $\hat{k} = k + n_1 Q_1 + n_2 Q_2$ where n_1, n_2 are the two integers which minimize $\|k + n_1 Q_1 + n_2 Q_2\|$. Here, we explicitly consider triangular and square symmetry of the supercell, so that $\{\hat{k}\}$ are inside an hexagon or a square, respectively. The Brillouin zone $\mathcal{B}(Q_1, Q_2)$ is the set of vectors \hat{k} for $k \in \mathcal{B}_0$. Further, we truncate the number of lattice vectors of the sub-lattice Λ and include only the first M_Λ vectors of smallest norm in the numerical calculations. In the framework of band structure calculations, where the Bloch states are obtained from an external periodic potential, M_Λ corresponds to the number of bands considered.

The Wigner crystal contains as many electrons as states in the Brillouin zone, corresponding to $\det(Q_1, Q_2) = (2\pi)^2 n$ for the fully polarized and $\det(Q_1, Q_2) = 2\pi^2 n$ for the unpolarized system. In units of k_F , setting $Q \equiv \|Q_1\| = \|Q_2\|$, we obtain $Q_W = \sqrt{2\pi/\sqrt{3}} \approx 1.9046$, for the triangular WC, whereas $Q_W = \sqrt{\pi} \approx 1.7725$ for the square WC. The FG can be formally regarded as $Q = \infty$, but the main region of interest within HF is smaller, $Q \leq 2$. In general, for $Q \neq Q_W$, the occupation of each point of the Brillouin zone can vary continuously, and the Hartree-Fock minimization

for incommensurate phases is a complicated combinatorial problem. Thus, we prefer to work with density matrices instead of single particle wave functions.

C. HF minimization using the single particle density matrix

The one body density matrix, ρ_1 , is a symmetric positive matrix $\rho_1(k\sigma, k'\sigma')$ with $\sigma, \sigma' = \pm$, such that $\text{Tr}\rho_1 = 1$. Provided that $\rho_1 < 1/N$, this matrix can be seen as one body density matrix of a state of N electrons. Within HF, the two body density matrix can be expressed in terms of ρ_1 ,

$$\rho_2(k_1\sigma_1, k_2\sigma_2; k'_1\sigma'_1, k'_2\sigma'_2) = \frac{N}{N-1}\rho_1(k_1\sigma_1, k'_1\sigma'_1)\rho_1(k_2\sigma_2, k'_2\sigma'_2) - \rho_1(k_1\sigma_1, k'_2\sigma'_2)\rho_1(k_2\sigma_2, k'_1\sigma'_1) \quad (2)$$

and the total energy, a-priori a function of the reduced one and two body density matrices, can be expressed entirely as a functional of ρ_1 . Explicitly, we obtain for the energy per particle:

$$E = \frac{1+\zeta}{r_s^2} \sum_{k \in L^*, \sigma} k^2 \rho_1(k, \sigma; k, \sigma) + \frac{\sqrt{2}}{4\pi r_s \sqrt{1+\zeta}} \sum_{q, k_1, k_2 \in L^* \atop \sigma_1, \sigma_2} v_q \times [\rho_1(k_1, \sigma_1; k_1 + q, \sigma_1)\rho_1(k_2, \sigma_2; k_2 - q, \sigma_2) - \rho_1(k_1, \sigma_1; k_2 - q, \sigma_2)\rho_1(k_2, \sigma_2; k_1 + q, \sigma_1)] \quad (3)$$

where all momenta are in units of k_F , $v_q = 2\pi/\|q\|$ for $q \neq 0$, and $v_0 = 0$. The unpolarized Fermi gas (U-FG) corresponds to $\rho_1(k\sigma, k'\sigma') = \delta_{kk'}\delta_{\sigma\sigma'}\chi_{\|k\|<1}/N$ with the corresponding energy $E_{FG}^U = 1/(2r_s^2) - 8/(3\pi\sqrt{2}r_s)$. Further, we also introduce the energy of the fully polarized Fermi gas (P-FG) with $\rho_1(k\sigma, k'\sigma') = \delta_{kk'}\delta_{\sigma+\delta_{\sigma\sigma'}\chi_{\|k\|<1}}/N$ as reference: $E_{FG}^P = 1/r_s^2 - 8/(3\pi r_s)$.

In the following we restrict the density matrix to represent commensurate and incommensurate periodic solutions. The corresponding one-body density matrix can be written as $\rho_k(q, q') = \rho_1(k+q, k+q')$ with $q, q' \in \Lambda$ and k in the Brillouin zone \mathcal{B} . Thus, the density matrix is now described by a family of positive matrices ρ_k such that $\rho_k < 1/N$ and $\sum_k \text{Tr}\rho_k = 1$. Note that the polarization of the electrons is not kept fixed and thus evolves to minimize the HF energy.

Numerically, we represent ρ_k as $U_k^* D_k U_k$ where D_k is a diagonal matrix with $0 \leq D_k \leq 1/N$ and U_k is a unitary matrix. For small r_s , the elements of the density matrix with high momenta, $\hat{k} + n_1 Q_1 + n_2 Q_2$, become negligible as n_1 or n_2 increases, and we include only the first M_Λ vectors in Λ . The potential energy contains a convolution in momentum space calculated using fast Fourier transform (FFT). The minimization of the HF energy is done computing the gradient of the energy with respect to U_k and D_k . The only drawback of the method is to fulfill the condition $\rho_k < 1/N$.

The minimization at given density consists in the following steps. At first we choose D_k and U_k to start with. Then we find the best U_k with a quadratic descent method¹⁰. The next step is to try to improve D_k given the gradient of the energy with respect to D_k and the linear constraints, $0 \leq D_k \leq 1/N$ and $\sum_k D_k = 1$. The process stops as soon as $D_k^{(\text{new})} = D_k$. In this case almost every D_k are 0 or $1/N$ and the gradient is negative or positive accordingly. Otherwise, we change D_k into $(1-\varepsilon)D_k + \varepsilon D_k^{(\text{new})}$ (with a small ε to ensure that U_k follows D_k *adiabatically*) and we restart the minimization with respect to U_k .

III. CONVERGENCE STUDIES

We first focus on size effects in the thermodynamic limit extrapolation, $N \rightarrow \infty$. From the relation $N/M_B = (Q_W/Q)^2$, this limit at fixed Q is equivalent to study the convergence with respect to $M_B = M^2$. Fig. 2 shows the size extrapolation of the P2DEG at $r_s = 4$ in the triangular Wigner crystal case, together with the results of Trail et al.¹³, done at $M_B = 13$ and $M_\Lambda \simeq 20$, and those of Ref.¹⁰. As the calculations of Ref.¹⁰ do not assume any periodicity in the HF search, they are limited to smaller systems $N \lesssim 500$, and the extrapolation to the thermodynamic limit is less accurate.

Size effects depend on the phase considered. In the incommensurate phase, size corrections are not any more monotonic functions, as in the Wigner crystal, but oscillatory behavior occurs depending on the density r_s , and on the modulation vector Q . In Fig.3, we show the energy of the P2DEG at $r_s = 2.5$ versus the modulation Q of the incommensurate crystal for various system sizes using $M = 2^p$, with p from 4 to 9 ($M_B = 16^2$ up to 512^2). Note the random like oscillations due to the discretization, M_B , of the Brillouin zone. However, with $M_B = 512^2$ for the P2DEG and $M_B = 2 \times 256^2$ for the U2DEG, these oscillations are sufficiently small to analyze safely $E(Q, r_s)$.

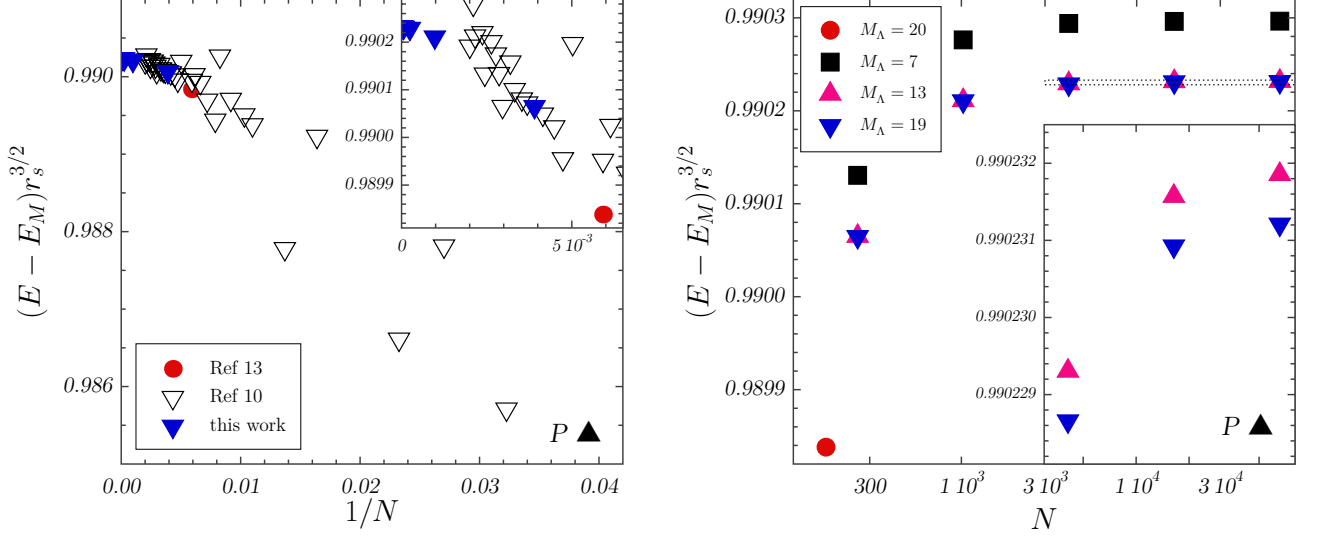


FIG. 2. (color on line) Energy (in Hartree units) of the P2DEG at $r_s = 4$ in the triangular Wigner crystal, as a function of the number of particles, $N \equiv M_B$, and the number of included bands, M_Λ . $E_M = -1.1061/r_s$ is the Madelung energy. Left: comparison with previous work^{10,13,15}. Blue full down triangles are results of the present work using $M_\Lambda = 19$. Right: convergence with respect to N and M_Λ . The inset is a zoom of the dotted-line-domain.

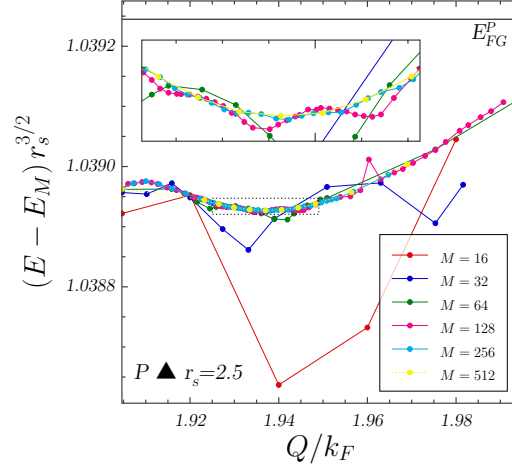


FIG. 3. Variation of the energy of the P2DEG at $r_s = 2.5$ with triangular symmetry versus Q for different values of $M_B = M^2$. Inset is the zoom of the region represented by the dashed rectangle.

Our second parameter is the number of vectors M_Λ considered in Λ . Note that truncation of Λ does not violate the variational principle, so that the energy of a converged HF solution must decrease as M_Λ increases. Figure 2 and Fig. 4 show the convergence in system size M_B (discretization of the Brillouin zone) together with the exponential convergence in M_Λ which measures the large k importance. As expected, energies decrease with M_Λ because the Hilbert space is increased. Interestingly, the M_Λ improvement is mainly independent of M_B (see Fig.2-right and Fig.4), which allows us to work with small M_Λ and estimate corrections using small systems. Most of the calculations presented in this paper are thus performed with $M_\Lambda = 7$ and $M_\Lambda = 9$ bands for supercells of triangular and square symmetry, respectively.

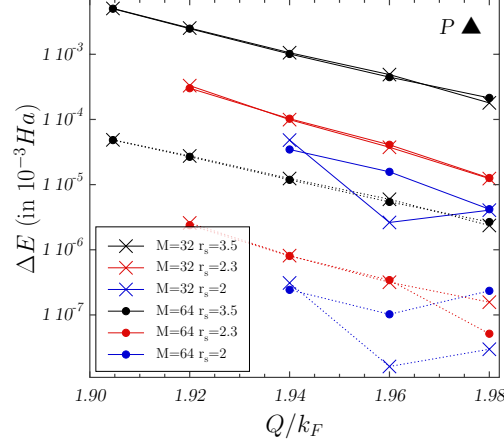


FIG. 4. (color on line) Convergence of the energy with respect to M_Λ for the P2DEG with triangular symmetry for two system sizes $M = 32$ and $M = 64$. Full and dotted lines stands $\Delta E = E_{M_{\Lambda_1}} - E_{M_{\Lambda_2}}$ and $\Delta E = E_{M_{\Lambda_2}} - E_{M_{\Lambda_3}}$, respectively, with $M_{\Lambda_1} = 7$, $M_{\Lambda_2} = 13$, $M_{\Lambda_3} = 19$. Crosses and dots stand for $M = 32$ and 64 , respectively. (Values at $r_s = 2$ are close to the convergence threshold of the descent method.)

IV. RESULTS

We have studied the HF ground state of the 2DEG in the density region $0.8 \leq r_s \leq 4$ at zero temperature considering commensurate and incommensurate solutions with square and triangular symmetries. At low densities the electrons form a commensurate Wigner crystal of modulations $Q = Q_W$ and we recover the results of previous HF studies^{10,13,15}. For higher densities, an incommensurate crystal with modulation $Q_W < Q < 2$ is formed for any fixed polarization and symmetry.

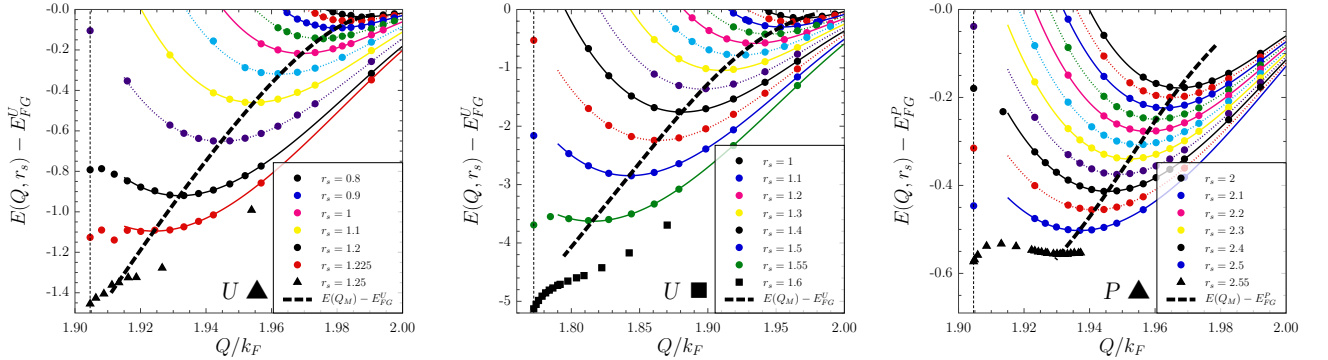


FIG. 5. Energy difference, with respect to the unmodulated Fermi gas, $E(Q, r_s) - E_{FG}^{U/P}$, in milli Hartree versus modulation, Q , for different densities, polarizations, and symmetry. (U▲): U2DEG with triangular symmetry, (U■): U2DEG with square symmetry (both for $N = 256$), (P▲) P2DEG with triangular symmetry ($N = 512$). Lines are the polynomial fits given in Table-I. In each figure, the lowest curves (largest r_s) with triangular or square symbols has a minimum at $Q = Q_W$. The bold dashed-line connects $Q_M(r_s)$, the minima of $E(Q, r_s)$ for fixed r_s . Vertical dotted lines indicate Q_W .

Figure 5 summarizes the energy gain with respect to the unmodulated Fermi gas as a function of Q at different densities. Well inside the incommensurate phase ($Q > Q_W$), the energies can be well represented with a polynomial

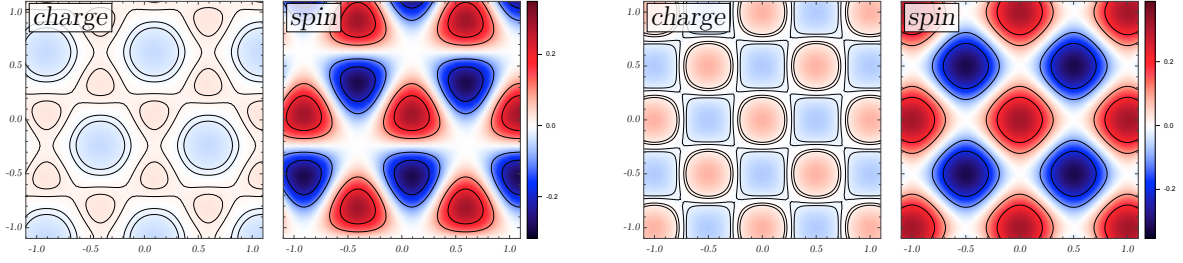


FIG. 6. (color on line) One body charge and spin densities in the triangular geometry (left: $r_s = 1.2$, $Q/k_F = 1.933$) and square geometry (right: $r_s = 1.5$, $Q/k_F = 1.844$). Average values have been subtracted. Lengths are given in units of the inverse modulation, Q^{-1} . The color scaling is the same for all pictures. Contour levels are at ± 0.1 , ± 0.2 for the spin densities and ± 0.01 , ± 0.02 for the charge densities.

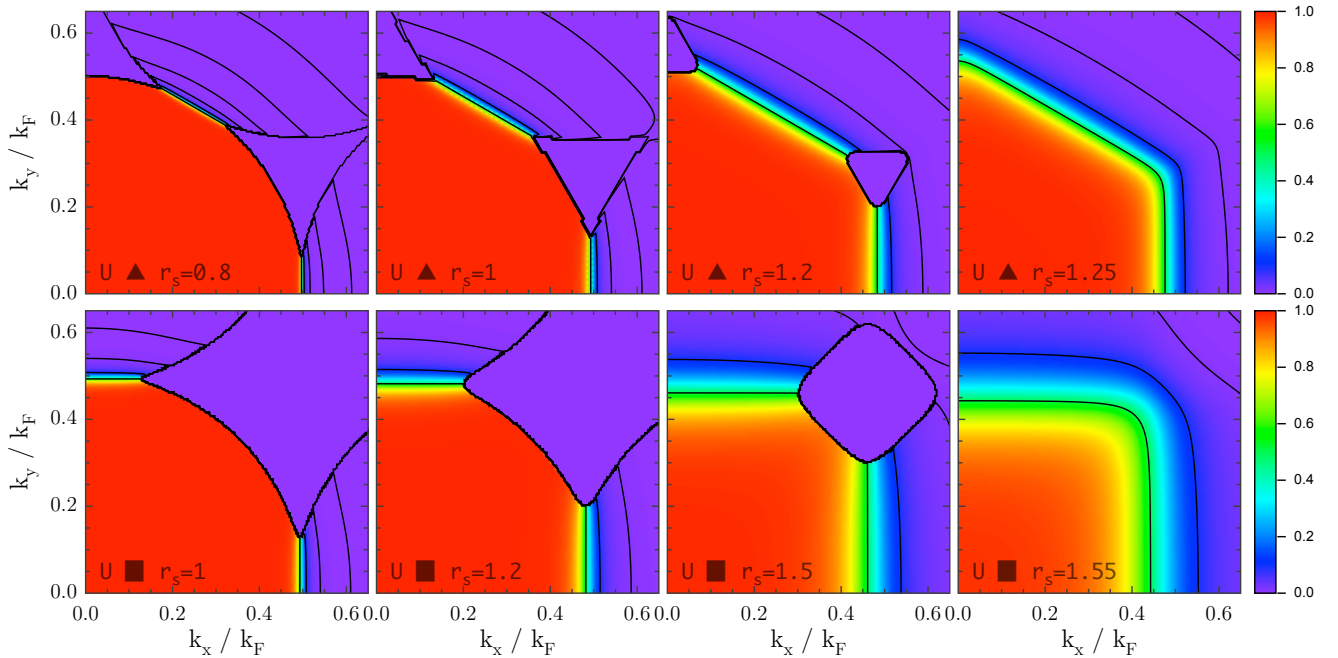


FIG. 7. (color on line) Modulus of the momentum distribution $|n_{\uparrow}(k)| = |n_{\downarrow}(k)|$ for the U2DEG in the positive quadrant (other parts can be deduced by symmetry). Top line and bottom line are for the triangular and square geometry, respectively. Contour levels are at 0.5 and 0.1, 0.01, etc. From right to left is shown the evolution from the Wigner crystal distribution (continuous function everywhere) to Fermi gas with a step along some directions. For the incommensurate states, note the step-function behavior to a domain where $n_k = 0$ which grows in the corner of the Brillouin zone when r_s decreases.

form:

$$E(Q, r_s) = E_{FG}(r_s) + \sum_{i=0}^3 \sum_{j=0}^2 \alpha_{ij} X^i r_s^j \quad (4)$$

where $X = 100(Q-2)$. The parameters α_{ij} determined by least square fits are given in Table-I. From this parametrization, for fixed r_s , we determine the minimum $Q_m(r_s)$ of $E(Q, r_s)$, shown in Fig.5.

The incommensurate phase is characterized by a crystal in direct space with slightly more lattice sites M_B than electrons N , increasing for larger modulation according to $M_B/N = (Q/Q_W)^2$. Figure 6 shows typical charge and spin densities in the incommensurate phase for the triangular and square geometry. The two examples are chosen close to the transition to the *Wigner* crystallization. The amplitude of the modulation of the charge densities is about an order of magnitude smaller than that of the spin densities, an effect which is even more pronounced at higher

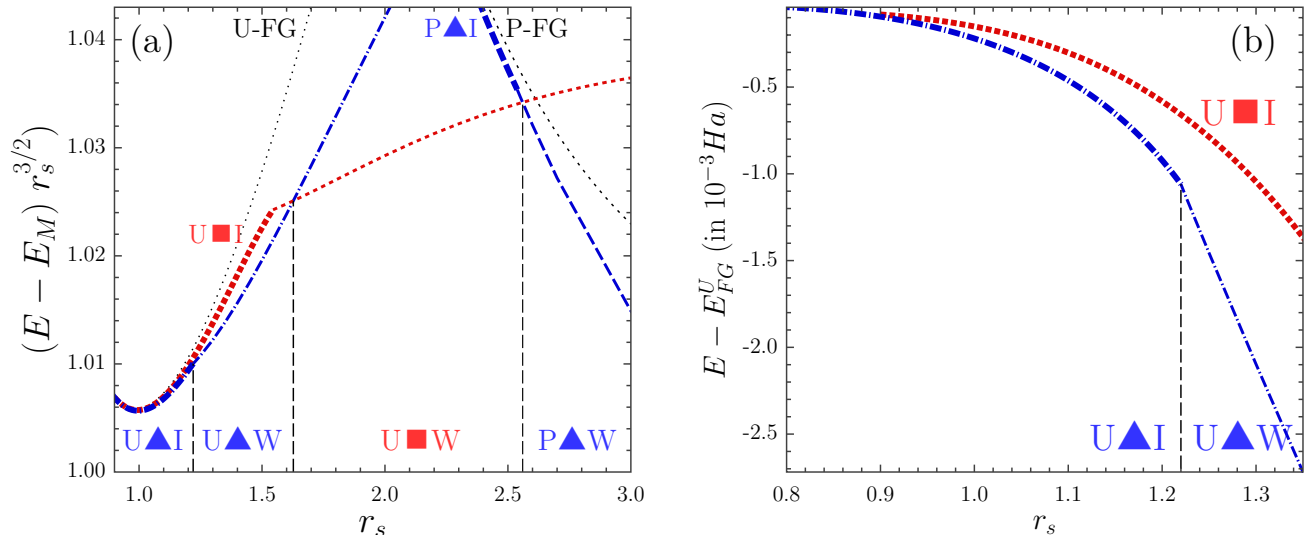


FIG. 8. (color online). (a): Phase Diagram of the 2DEG at $T = 0$. $E_M = -1.1061/r_s$ is the Madelung energy. Dotted lines correspond to the Fermi gas. Blue and red curves represent the triangular and square phases. P and U stand for polarized and unpolarized, respectively. W and I (thick curves) stand for Wigner and Incommensurate crystal, respectively. The dashed vertical lines indicate the transitions. (b): zoom of part of (a) with an another energy reference.

density.

The momentum distribution n_k (N times the diagonal part of ρ_1) provides additional insight. In contrast to the step-function behavior at k_F of the Fermi gas, n_k is continuous inside the commensurate Wigner crystal phase and its variation reflects the symmetry of the Brillouin zone. The incommensurate phase still reflects the underlying symmetry of the crystal, but angle selective steps occur at the corners of the Brillouin zone (see Fig. 7). The rounding of the corners increases for smaller r_s , and the isotropic step-function of the Fermi gas is continuously approached for $r_s \rightarrow 0$.

Whereas we have found that the incommensurate phase is always favored compared to the Fermi gas solution, independently of the imposed polarization and crystal symmetry, the unpolarized incommensurate hexagonal crystal becomes the true HF ground state at high densities, $r_s \leq r_s^c \simeq 1.22$. The different phases and energies for $0.8 \leq r_s \leq 4.0$ are illustrated in Fig. 8. Although our HF method does not impose the polarization, we have not found any stable partially polarized ground states. At $r_s > r_s^c$ the unpolarized electrons form a commensurate Wigner crystal of hexagonal symmetry, and, at $r_s \simeq 1.62$ a structural transition from the unpolarized hexagonal WC to the unpolarized square WC occurs, followed by a first order transition to the polarized triangular WC at $r_s \simeq 2.6$.

V. CONCLUSION

We have studied the 2DEG in the Hartree-Fock approximation at densities $r_s \lesssim 4$. We confirm previous observations of incommensurate phases of the fully polarized electron gas¹⁰, performing calculations of much larger system sizes. We further included electron polarization, as well as square and triangular symmetries. Our HF phase diagram at zero temperature is much richer than that obtained previously¹³, which did not consider the unpolarized triangular WC, nor any incommensurate phase. Our numerical calculations explicitly confirm the old conjecture of Overhauser^{8,9} that Fermi gas is never the HF ground state which has been proven rigorously for the fully polarized electron gas¹⁰.

We have further shown that the momentum distribution provides an unambiguous characterization of the incommensurate phase. In contrast to the isotropic momentum distribution of a Fermi liquid, discontinuous at the Fermi surface^{16,17}, the incommensurate phase exhibits an anisotropic momentum distribution intermediate between a crystal and the Fermi gas with forbidden domains inside the Brillouin zone, where n_k jumps to zero.

TABLE I. Coefficients α_{ij} of the polynomial fits $E(Q, r_s) - E_{FG}(r_s)$ defined by Eq.4 for the P2DEG in the triangular geometry and the U2DEG for the square and triangular geometry.

P-Triangular			U-Square			U-Triangular		
0.15758	-0.08577	-0.011495	-0.621900	1.53040	-0.96941	-0.78611	1.88240	-1.13180
0.24875	-0.24028	0.070520	0.058858	-0.26652	0.27359	0.35614	-0.64435	0.34780
0.11155	-0.10668	0.024822	0.032321	-0.06425	0.025000	0.10624	-0.15804	0.05531
-0.00090	-0.00321	0.001310	-0.022986	0.02665	-0.00750	-0.00166	-0.00044	0.00081

-
- ¹ S. Huotari, J. A. Soiminen, T. Pylkkänen, K. Hämäläinen, A. Issolah, A. Titov, J. McMinis, J. Kim, K. Esler, D. M. Ceperley, M. Holzmann, and V. Olevano, Phys. Rev. Lett. **105**, 086403 (2010).
² T. Ando, A.B. Fowler, and F. Stern, Rev. Mod. Phys. **54**, 437 (1982).
³ E. P. Wigner, Trans. Faraday Soc. **34**, 678 (1938); Phys. Rev. **46**, 1002 (1934).
⁴ D. M. Ceperley and B. J. Alder, Phys. Rev. Lett. **45**, 566-569 (1980).
⁵ Candido, L., B. Bernu and D. M. Ceperley, Phys. Rev. B **70**, 094413:1-6 (2004).
⁶ B. Tanatar and D.M. Ceperley, Phys. Rev. B **39**, 5005 (1989).
⁷ L. Cândido, B. Bernu, and D.M. Ceperley, Phys. Rev. **B 70**, 094413 (2004).
⁸ A. W. Overhauser, Phys. Rev. Lett. **4**, 462 (1960); Phys. Rev. **128**, 1437 (1962).
⁹ G. F. Giuliani and G. Vignale, *Quantum Theory of the Electron Liquid*, Cambridge University Press, Cambridge (2005).
¹⁰ B. Bernu, F. Delyon, M. Duneau, and M. Holzmann, Phys. Rev. B **78**, 245110 (2008); cond-mat/0810.3559.
¹¹ B. Spivak and S.A. Kivelson, Phys. Rev. **B 70**, 155114 (2004).
¹² H. Falakshahi and X. Waintal, Phys. Rev. Lett. **94**, 046801 (2005), X. Waintal, Phys. Rev. **B 73**, 075417 (2006).
¹³ J. R. Trail, M. D. Towler, and R. J. Needs, Phys. Rev. **B 68**, 045107 (2003).
¹⁴ S. Zhang and D. M. Ceperley, Phys. Rev. Lett. **100**, 236404 (2008), arXiv:0712.1194 (2007).
¹⁵ Using the same parameters, we recover exactly the results of Trail et al.¹³ for the P2DEG at $r_s > 3$. We thank the authors for sending us their data.
¹⁶ M. Holzmann, B. Bernu, V. Olevano, R. M. Martin, and D. M. Ceperley, Phys. Rev. B **79**, 041308 (2009).
¹⁷ M. Holzmann, B. Bernu, C. Pierleoni, J. McMinis, D.M. Ceperley, V. Olevano, and L. Delle Site, arXiv:1105.2338 (2011).